Computers and Geotechnics 96 (2018) 25–39

Contents lists available at ScienceDirect

Computers and Geotechnics

journal homepage: www.elsevier.com/locate/compgeo

Research Paper

Numerical evaluation of reinforced slopes with various backfill-reinforcement-drainage systems subject to rainfall infiltration

Kuo-Hsin Yang[a,*], Joseph Ng'ang'a Thuo[b], Vo Duyen Anh Huynh[c], Thanh Son Nguyen[d], Fernando Henrique Martins Portelinha[e]

[a] Department of Civil Engineering, National Taiwan University (NTU), 1, Sec. 4, Roosevelt Rd., Taipei 106, Taiwan
[b] Department of Civil Engineering, Dedan Kimathi University of Technology, Kenya
[c] Department of Civil Engineering, The University of Da Nang, Viet Nam
[d] Department of Civil and Construction Engineering, National Taiwan University of Science and Technology (Taiwan Tech), Taipei, Taiwan
[e] Department of Civil Engineering, Federal University of Sao Carlos, Sao Carlos, Brazil

ARTICLE INFO

Keywords:
Geosynthetics
Unsaturated backfill
Sand cushion
Slope stability
Suction
Rainfall infiltration

ABSTRACT

This paper presents a numerical study investigating the hydraulic response and stability of geosynthetic-reinforced soil slopes subject to rainfall. A series of numerical simulations of unsaturated slopes with various backfill–reinforcement–drainage systems subject to rainfall infiltration was performed by comprehensively considering the combined effect of backfill (i.e., sand, silt, and silty clay), reinforcement type (i.e., geogrid or nonwoven geotextile), and rainfall intensity (350 and 500 mm/day). The backfills were modeled using three soil–water characteristic curves (SWCCs) representing the general suction range associated with sand, silt, and clay. The influence of sand cushions in improving the stability of reinforced clay slopes was also assessed. The numerical results reveal that the loss of matric suction and development of a capillary barrier effect within clay backfills could have adverse impacts on both the global and local stabilities of the reinforced clay slopes. The contribution of matric suction in enhancing slope stability was initially high for reinforced clay slopes; however, the global stability of the reinforced clay slope substantially decreased due to the loss of matric suction as the rainfall infiltration proceeded. The local instability of the geotextile-reinforced clay slope occurred due to the capillary barrier effect at the geotextile–clay interface. The reinforced marginal soil slopes cannot effectively drain the infiltrating water under torrential rainfall. Free drainage conditions may not be assumed for these slopes if the drainage is not properly considered. Both the global and local factors of safety (FS) of the reinforced sand slope were minimally influenced by the loss of matric suction induced by rainfall infiltration. The required reinforcement tensile strengths for the reinforced silt and clay slopes to maintain $FS = 1.3$ were, respectively, approximately 3 and 4 times larger than that for reinforced sand slopes. Numerical results also indicated that the inclusion of sand cushions, which provide both strength and drainage functions, can effectively enhance the slope stability. An optimal sand cushion thickness of 15 cm (replacing 20% of marginal backfill with sand) was determined in this study.

1. Introduction

Geosynthetic-reinforced soil (GRS) structures are typically composed of four components: soil, reinforcement, facing, and drainage. Each component has various material options that can have different influences on the performance of the GRS structure. Considering backfill types as an example, design guidelines [1,5,12,39] recommend the use of coarse-grained soils as a backfill material within the reinforced zone. However, fine-grained backfill soils (referred to as marginal fills), which are often locally available and provide both economic and sustainability benefits, have gained increasing popularity as an alternative to high-quality granular fills [4,42,45,51,65]. The contrasting merits and demerits of using marginal fills have been reported and discussed.

Positive aspects of using locally available marginal fills are reducing transport costs and minimizing environmental impacts associated with the disposal of excavated soils. In addition, because the backfills are usually compacted within ± 2% of optimum moisture content, the

* Corresponding author.
E-mail addresses: khyang@ntu.edu.tw (K.-H. Yang), joseph.thuo@dkut.ac.ke (J.N. Thuo), hvdanh@dct.udn.vn (V.D.A. Huynh), sonnt@nuce.edu.vn (T.S. Nguyen), fportelinha@ufscar.br (F.H.M. Portelinha).

http://dx.doi.org/10.1016/j.compgeo.2017.10.012
Received 20 June 2017; Received in revised form 14 October 2017; Accepted 22 October 2017
Available online 02 November 2017

matric suction generated within unsaturated fills could exert favorable effects on reinforced soil structures [30,53,54]. Matric suction plays a crucial role in the interparticle or effective stress state of unsaturated soils [14,19,33,48,54,63]. The presence of suction can increase soil effective stress and thus enhance the performance and stability of reinforced soil structures by increasing soil stiffness and shear strength [13,19,27], increasing soil–reinforcement interface strength [4,41,65], and reducing mobilized reinforcement load [25,46,54].

The key criticism of the use of marginal fills concerns the uncertainty and variation of porewater pressure (PWP) within reinforced zones subjected to various moisture conditions. Some fine-grained soils with a low drainage capacity have been observed to compromise the performance of reinforced soil structures upon rainfall infiltration owing to the development of a positive PWP [8,26,28,32,35,56,61,65]. Despite this fact, studies have demonstrated that the problem of PWP accumulation within marginal fills can be appropriately alleviated by installing sufficient and efficient drainage [10,38,41,44].

In addition to backfill types, the influence of reinforcement types (i.e., geogrid or geotextile) on the performance and stability of reinforced structures has been discussed in the literature. In addition to reinforcement function, nonwoven geotextiles are expected to provide drainage functions to facilitate PWP dissipation within saturated backfills [15,18,41,43,44]. However, studies have reported that, under unsaturated soil conditions, nonwoven geotextiles can retard water flow due to the capillary barrier effect [15,25,36,42,64]. Because of the capillary barrier effect, a measurable amount of water does not flow from the backfill soil to the underlying nonwoven geotextile drain until a critical suction threshold is achieved; hence, nonwoven geotextile may act as a water barrier instead of a drainage material and lead to an increase in PWP in the soils immediately above it. Bouazza et al. [7] and Iryo and Rowe [23] suggested that considerable care is required when selecting nonwoven geotextiles for use within soil structures in order to avoid increased PWP developing.

The preceding discussion explains the dilemma of selecting backfill and reinforcement for GRS structures and describes the complex interaction and mutual influence between backfill–reinforcement–drainage systems in GRS structures. Few studies on the overall evaluation of such systems have been published. Accordingly, this study addressed this concern by performing a series of numerical analyses to investigate the hydraulic response and stability of reinforced slopes subject to rainfall by comprehensively considering the combined effect of backfill (i.e., sand, silt, and silty clay) and reinforcement types (i.e., geogrid or nonwoven geotextile) and rainfall intensity (350 and 500 mm/day). The study findings can facilitate developing improved methodologies for the analysis and design of reinforced soil structures constructed using marginal soils and can provide suitable guidance for selecting an appropriate backfill–reinforcement–drainage system for GRS structures. The specific objectives of this study were as follows: 1. to assess the rainfall-induced suction variation in reinforced slopes with various backfill–reinforcement–drainage systems; 2. to examine the influence of suction variation on both the global and local stability of reinforced slope systems; and 3. to evaluate the required reinforcement tensile strength to achieve a consistent stability level for the reinforced slopes with various backfills under specified rainfall conditions.

This study also assessed the effectiveness of sand cushions, granular soil-layer sandwiching reinforcement and drain layers, in improving the drainage and stability of reinforced marginal soil slopes. Fig. 1 illustrates the application of granular soils as facing drains and sand cushions in a GRS structure in current practice. Studies have demonstrated that the application of sand cushions can accelerate PWP dissipation under saturated conditions [43,44], reduce the capillary barrier effect under unsaturated conditions [51], mitigate the surficial intrusion and long-term clogging in nonwoven geotextiles by fine-grained soils [9,31], enhance pullout resistance [3], and improve the strength and deformation characteristics of reinforced clay by improving the soil–reinforcement interface shear strength [2,52,60]. In this study, the influence of the use of sand cushions in improving the stability of reinforced slopes was assessed, and the contribution of sand cushions resulting from their strength and drainage functions was quantified. The optimal thickness of the sand cushions was also determined.

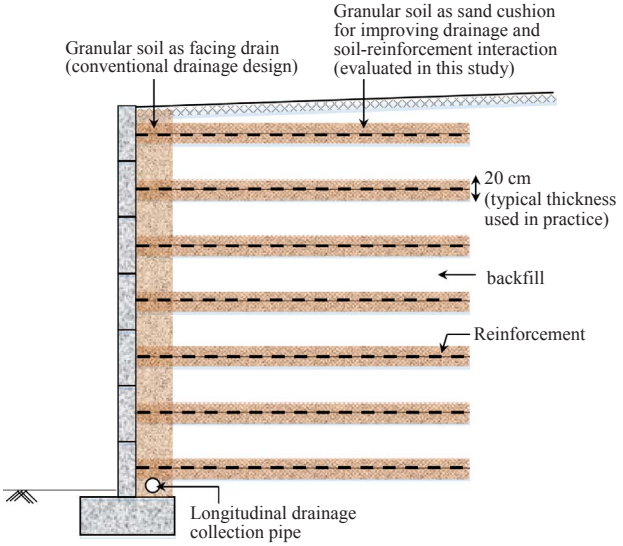

Fig. 1. Illustration of application of granular soils as facing drain and sand cushion in a geosynthetic-reinforced soil structure in current practice.

2. Numerical analysis of reinforced slope

2.1. Numerical model and verification

Numerical analyses were performed to investigate the hydraulic response and stability of reinforced slopes with various soil–reinforcement–drainage systems subject to rainfall. Two-dimensional embankment models (Fig. 2) were developed using SEEP/W and SLOPE/W software [16,17]. The numerical models were established on the basis of the full-scale embankment model tests conducted by the Public Works Research Institute (PWRI), Japan, reported by [25]. The embankments were 3 m high and 6 m long, with a slope of 0.7H:1V (= 55°). Four layers of geosynthetic reinforcements were placed with a vertical spacing of 0.75 m. A flow flux was specified as the boundary condition on the top and side slope surfaces of the embankment to model rainfall infiltration.

The validation of the numerical model was reported by the authors in a companion paper [51]. A reasonably good agreement was achieved between the measured and numerical results of PWP distribution within the embankment. In addition, the authors demonstrated that numerical analysis is capable of capturing the capillary barrier effect at the soil–geotextile interface. Notably, this companion paper [51] primarily investigated the influence of the capillary barrier effect on nonwoven geotextile-reinforced soil slopes, whereas the present study comprehensively evaluated the complex interaction and mutual influence among various backfill–reinforcement–drainage systems.

In this study, a series of numerical reinforced slope models with various backfill–reinforcement–drainage systems was established (Fig. 2). Numerical investigation was conducted by considering various types of backfills (sand, silt, and silty clay) and geosynthetic reinforcements (geogrid and nonwoven geotextile). Sand represents a good-quality backfill, and silt and silty clay represent marginal backfills with different fine contents. For modeling geosynthetics, the geogrid provides only the reinforcement function, whereas nonwoven geotextile is equipped with both reinforcement and drainage functions. The 3-mm thick nonwoven geotextile was modeled using six-node triangular elements with prescribed hydraulic properties across the thickness of the

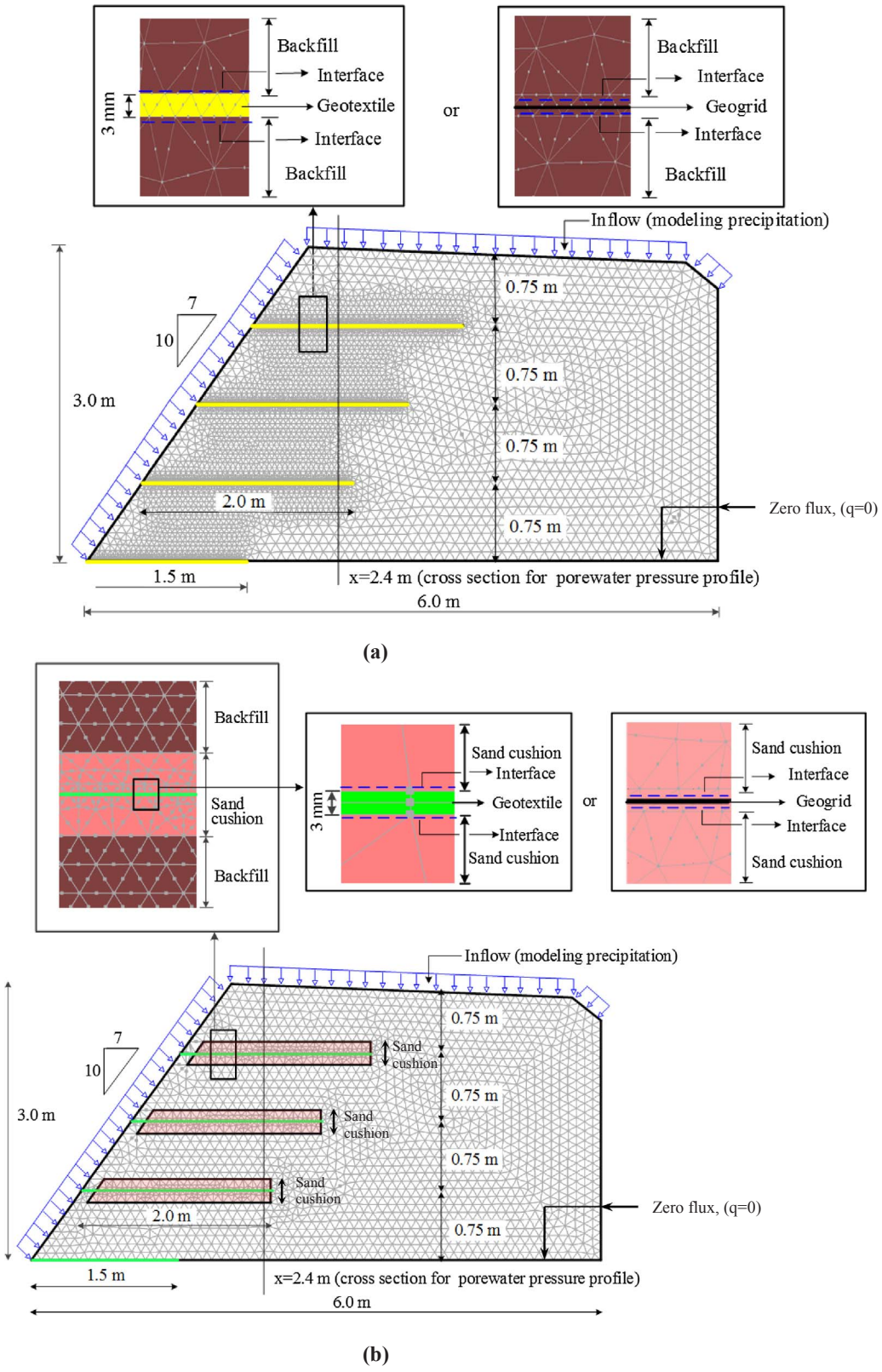

Fig. 2. Numerical models: (a) geotextile- or geogrid-reinforced slope; (b) reinforced slope with sand cushions.

geotextile. The geotextile-reinforced slopes were modeled using 4668 six-node triangular elements, whereas the geogrid-reinforced slopes were modeled using 3396 six-node triangular elements.

In the case of reinforced slopes with sand cushions (Fig. 2b), the geosynthetics were sandwiched between sand layers (on the top and bottom of the geosynthetics). The sand cushion layers were placed 15 cm away from the slope face to prevent the water from directly entering into the slope. The thickness of the sand cushions was varied from t_s = 0 to 35 cm to evaluate the influence of sand cushion thickness in improving the stability of the reinforced clay slopes.

2.2. Input material properties

The backfills were modeled using three soil–water characteristic curves (SWCCs), adopted from Zhang et al. [63], to represent the general suction range associated with sand, silt, and silty clay. The water retention curve (WRC) of the nonwoven geotextile was deduced from Iryo and Rowe [24]. In this study, van Genuchten–Mualem's model [59] was applied to define the relationship between matric suction and volumetric water content and to estimate the changes in hydraulic conductivity with matric suction, expressed as follows:

$$\Theta = \frac{\theta-\theta_r}{\theta_s-\theta_r} = \left[\frac{1}{1+\{\alpha(u_a-u_w)\}^n}\right]^{1-1/n} \quad (1)$$

$$k_{rel} = \frac{k}{k_s} = \Theta^{1/2}[1-(1-\Theta^{1/(1-1/n)})^{1-1/n}]^2 \quad (2)$$

where Θ is the normalized volumetric water content; θ_s is the saturated volumetric water content; θ_r is the residual volumetric water content; $(u_a - u_w)$ is the matric suction (where u_a and u_w are the pore air and porewater pressures, respectively); α and n are the curve fitting parameters in van Genuchten-Mualem's model; k_{rel} is the relative hydraulic conductivity; k is the hydraulic conductivity at any soil degree of saturation; and k_s is the saturated hydraulic conductivity. Fig. 3 presents the hydraulic characteristics of the backfills and nonwoven geotextile. Table 1 summarizes the curve-fitting parameters and saturated hydraulic conductivities of backfills and the nonwoven geotextile obtained using van Genuchten–Mulem's model [59].

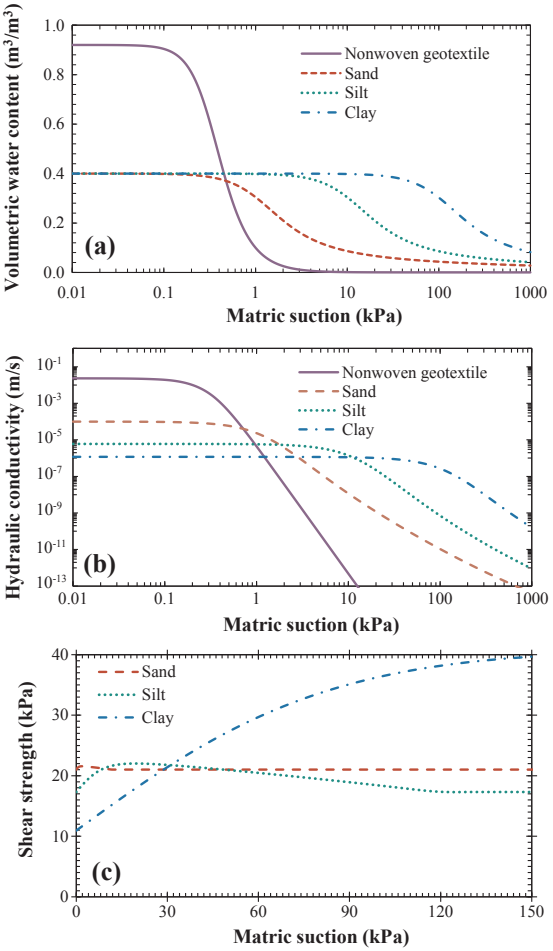

Fig. 3. Hydraulic characteristics and shear strength curves of sand, silt, clay, and geotextile: (a) water retention curves; (b) hydraulic conductivity functions; (c) soil shear strength.

Table 1
Hydraulic characteristic parameters for soils and nonwoven geotextile.

Material	θ_s	θ_r	α (kPa^{-1})	n	k_s (m/s)
Geotextile	0.92	0.00	3.0	3.0	2.30×10^{-2}
Sand	0.40	0.03	1.0	1.8	1.00×10^{-4}
Silt	0.40	0.04	0.1	2.0	6.00×10^{-6}
Clay	0.40	0.05	0.01	2.0	1.18×10^{-6}

The unsaturated soil shear strength was calculated using the extended Mohr–Coulomb criterion proposed by Vanapalli et al. [57]:

$$\tau = c' + (\sigma_n - u_a)\tan\phi' + \Theta(u_a - u_w)\tan\phi' \quad (3)$$

where τ represents soil shear strength; c' is the effective cohesion; ϕ' is the effective friction angle; and σ_n is the total normal stress on the failure plane; the rest of parameters have been defined earlier. By comparing Vanapalli's equation (Eq. (3)) with numerous unsaturated soil shear strength equations, Zhang et al. [63] found that it can efficiently describe and predict the nonlinear relationship between soil strength and matric suction. Furthermore, the applicability of Eq. (3) to predicting the failure loadings of shallow foundations on variably saturated soils was validated by Oh and Vanapalli [40], Vanapalli and Mohamed [58] and Vahefifard and Robinson [55].

To evaluate the local stability against soil interlayer sliding, the soil–reinforcement interface shear strength was considered in the simulation. The interface efficiencies ($=\tan\delta'/\tan\phi'$) were assumed to be $R_{inter} = 0.9$, 0.7, and 0.5 for the sand–reinforcement, silt–reinforcement, and clay–reinforcement interfaces based on the values reported by Eigenbrod and Locker [11], Koutsourais et al. [29], Martin et al. [34], and Zornberg et al. [66]. Similar to Eq. (3), the unsaturated interface shear strength was calculated as follows:

$$\tau = c_a' + (\sigma_n - u_a)\tan\delta' + \Theta(u_a - u_w)\tan\delta' \quad (4)$$

where τ represents soil-reinforcement interface shear strength; c_a' is the interfacial cohesion; and δ' is the interfacial friction angle; the rest of parameters have been defined earlier. Eq. (4) was used by Hamid and Miller [20] to evaluate the shear strength of unsaturated soil interfaces. Studies have reported the influence of matric suction on the soil–reinforcement interface shear strength. Hatami and Esmaili [67] conducted a series of pullout and interface shear tests to investigate unsaturated marginal soil–geotextile behavior. The test results suggested that the soil–reinforcement interface shear strength increased with the increase in soil matric suction. Hatami et al. [21] constructed a series of reduced-scale unsaturated embankment tests. The embankments were constructed using lean clay that had been compacted to with different water contents (i.e., optimum moisture content OMC and OMC ± 2%). The embankments were subjected to strip loading at the top, and the observed failure mode was the direct shear sliding of a block of soil over the top reinforcement layer. The test results confirmed that higher matric suction in drier soils yielded higher soil–reinforcement interface shear strength and consequently resulted in higher stability embankments that can bear relatively high failure loads.

Table 2 summarizes the input soil and soil–reinforcement interface shear strength properties. The soil unit weight was input as $\gamma = 17$ kN/m^3 for all backfills, and the effective friction angles of sand, silt, and

Table 2
Soil and soil-geosynthetic interface shear strength parameters.

Soil type	Unit weight γ (kN/m^3)	Effective friction angle ϕ' (°)	Interface reduction factor R_{inter}	Interface friction angle δ' (°)
Sand	17	35	0.9	32.2
Silt	17	30	0.7	22.0
Clay	17	20	0.5	10.3

Table 3
Numerical program of reinforced slopes with various backfill-reinforcement systems.

Slope	Backfill	Rainfall intensity					
		Torrential rainfall q = 350 (mm/day) = 4.05×10^{-6} (m/s)			Extremely torrential rainfall q = 500 (mm/day) = 5.79×10^{-6} (m/s)		
		q/k_s	Geotextile-reinforced	Geogrid-reinforced	q/k_s	Geotextile-reinforced	Geogrid-reinforced
1	Sand	0.04	1-A	1-B	0.06	1-C	1-D
2	Silt	0.68	2-A	2-B	0.96	2-C	2-D
3	Clay	3.50	3-A	3-B	4.90	3-C	3-D

clay were assumed to be $\phi' = 35^\circ$, 30°, and 20°, respectively. The effective cohesion was assumed to be $c' = 0$ kPa for all backfills because it is common in practice to ignore any cohesive strength component of soil strength if it is present [5,12]. Notably, despite the assumption that $c' = 0$, the apparent cohesion contingent on the soil suction was considered in the simulation [the term $\Theta(u_a - u_w)\tan\phi'$ in Eq. (3)]. Sand cushions have the same mechanical and hydraulic properties as sand backfills. Fig. 3c presents the variation in soil shear strength with matric suction under σ_n = 30 kPa, which corresponds to the overburden pressure at the mid-slope. Matric suction clearly had a significant influence on the shear strength of clay (shear strength changed from 11 to 40 kPa when matric suction varied from 0 to 150 kPa), whereas it had a negligible influence on the shear strength of sand.

2.3. Numerical program and simulation details

Table 3 summarizes the numerical program for modeling the unsaturated reinforced slopes with various backfill–reinforcement–drainage systems. Table 4 presents the numerical program of reinforced clay slopes with various sand cushion thicknesses. A total of 20 simulation cases were conducted. For each case, transient seepage analysis and limit equilibrium (LE) analysis were performed. The PWPs calculated from the transient infiltration analysis were input into the LE analysis to calculate the soil effective stress and the corresponding factor of safety (FS). In the LE analysis, both global (overall slope failure) and local (soil interlayer sliding above the topmost geosynthetic layer) stabilities were analyzed. The PWP profile and global and local FSs of each case were compared in this study.

In the transient seepage analysis, the governing equation for transient flow within an unsaturated medium was derived by Richards [47] from Darcy's law and the continuity equation.

$$k_x \frac{\partial^2 h}{\partial x^2} + k_y \frac{\partial^2 h}{\partial y^2} = \frac{\partial \theta}{\partial t} = m_w \gamma_w \frac{\partial h}{\partial t} \quad (5)$$

where h = total hydraulic head; k_x = unsaturated hydraulic conductivity in the x direction; k_y = unsaturated hydraulic conductivity in the y direction; m_w = coefficient of water volume change (slope of the water characteristics curve); γ_w = unit weight of water; and θ = volumetric water content.

Table 4
Numerical program of reinforced clay slopes with various sand cushion thickness.

Sand cushion thickness (cm)	Clay backfill Rainfall intensity, q = 350 (mm/day)	
	Geotextile-reinforced	Geogrid-reinforced
0	3-A	3-B
5	3-A-5	3-B-5
15	3-A-15	3-B-15
25	3-A-25	3-B-25
35	3-A-35	3-B-35

Initial suction values of −3.5, −12, and −100 kPa were specified for sand, silt, and silty clay, respectively. These values were obtained on the basis of the typical value of the as-compacted optimum water content of each backfill [22] and the corresponding SWCC in Fig. 3a. The importance of setting antecedent hydrology in numerical analysis has been discussed in many studies [6,37,50,62].

During the transient seepage analysis, rainfall intensities of q = 350 (i.e., 4.05×10^{-6} m/s) or 500 mm/day (i.e., 5.79×10^{-6} m/s), representing torrential rainfall and extremely torrential rainfall as defined by Taiwan Weather Bureau, were prescribed on the top and side surfaces of the embankments for a period of 24 h. The selected rainfall intensity, q = 500 mm/day, also reflects the extreme weather events that have recently occurred in Taiwan during the typhoon and East Asian monsoon season due to the influence of global warming. An impervious boundary was prescribed at the bottom of the slope to model an RC or well-compacted foundation. The prescribed impervious boundary also allows the influence of the build-up of a positive PWP from the bottom of the slope to be examined.

To allow seepage flowing out of the slope, once PWP became positive at any node on the top and side slope surfaces, the boundary condition was switched from the flux-specified boundary condition (i.e., q = 350 or 500 mm/day) to a pressure-head-specified boundary condition (h_p = 0 m). Surface runoff was permitted when the developed PWP on the slope surface changed to a positive value. An automatically adjusted time-step increment between 1 and 100 s was selected for attaining convergence.

In the LE analyses, slope stability calculations were performed using Spencer's method [49], which rigorously satisfies all equilibrium conditions (i.e., vertical force, horizontal force, and moment equilibrium). An allowable long-term tensile strength of T_a = 21.6 kN/m adopted from [25] was input for both the geotextile and geogrid. The same tensile strength values were selected for both the geotextile and geogrid with the intention of evaluating the difference between the calculated FSs caused by the drainage function of geosynthetics (only geotextile has a drainage function). The reinforcement force was assumed to be uniformly distributed with depth and to act horizontally on the failure surface (as-installed). The global FS for the entire slope and the local FS for the interlayer soil sliding along the top reinforcement layer were analyzed. By selecting the "optimization" function in Slope/W, multiple circular/noncircular slip surfaces were automatically searched until the critical failure surface corresponding to the minimum FS was identified.

3. Results and discussion

3.1. Moisture migration and porewater pressure profile

Fig. 4 presents the PWP profiles at a distance of x = 2.4 m from the toe of the slope under torrential rainfall conditions (q = 350 mm/day), corresponding to the following timings: 1. the initial condition (t = 0 h); 2. the wetting fronts were temporarily halted and the maximum PWP developed within the soil immediately above the topmost nonwoven geotextile layer (i.e., t = 3.5, 4.1, and 5.6 h for the reinforced sand, silt, and clay slopes, respectively); 3. the wetting front reached the bottom of the slope; and 4. the minimum global FS was obtained (either under steady-state seepage conditions or at the end of the rainfall event at t = 24 h). The hydrostatic line is also depicted in the figures for reference.

When the wetting front advanced downward, PWP increased from the initial values (−3.5, −12, and −100 kPa) to −2.0, −5.0, and 0 kPa at the top of the reinforced sand, silt, and clay slopes, respectively. Compared with sand and silt, the clay backfills in Slopes 3-A and 3-B experienced greater loss of matric suction after the wetting front passed. When the wetting front reached the bottom of the slope, the sand and silt backfills remained unsaturated, whereas the clay backfills became completely saturated (Fig. 4). This phenomenon can be evaluated using the ratio of rainfall intensity to saturated soil hydraulic

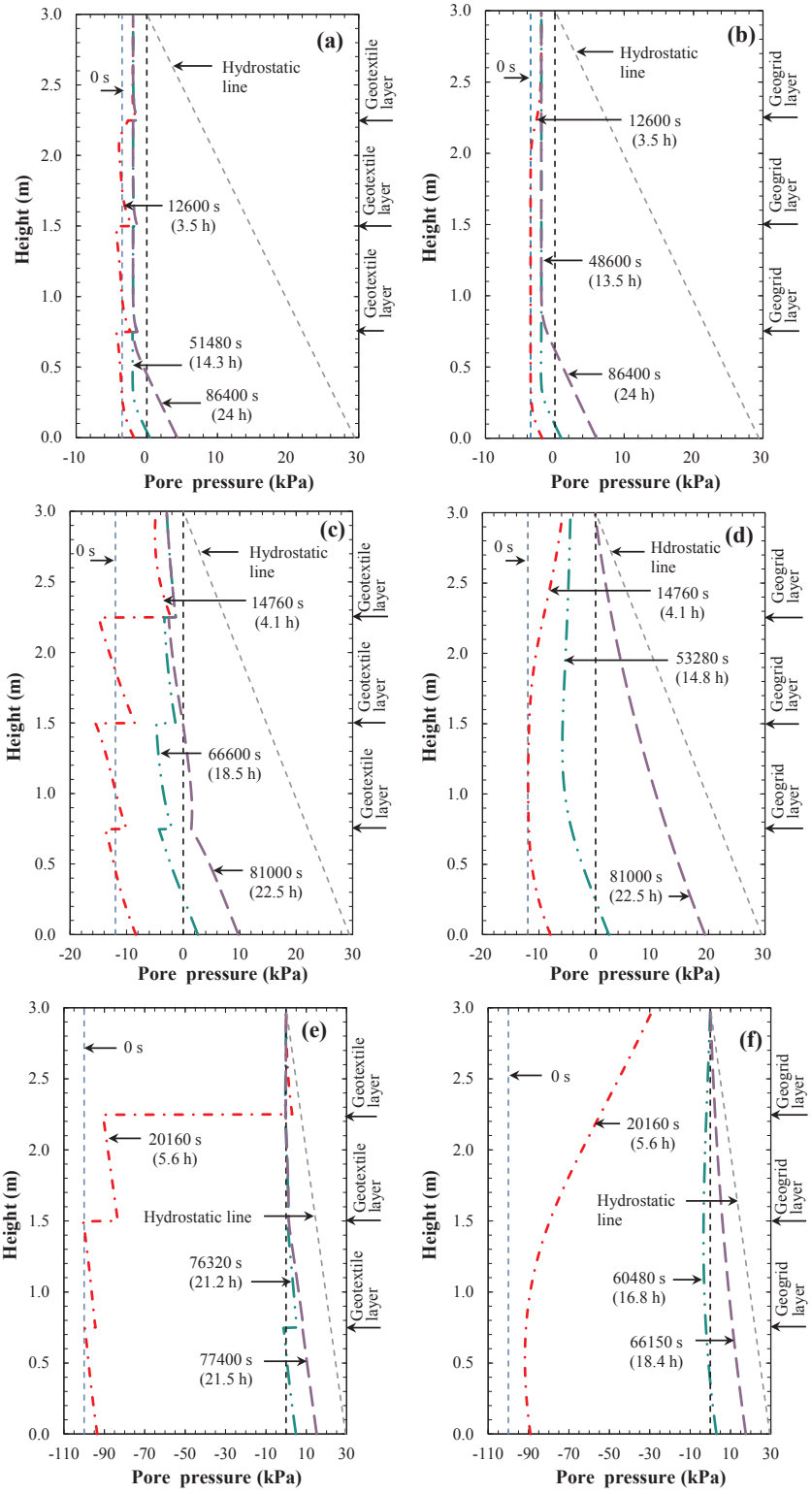

Fig. 4. Porewater pressure profile at a distance of $x = 2.4$ m from the toe of slopes under $q = 350$ mm/day: (a) Slope 1-A (sand-geotextile); (b) Slope 1-B (sand-geogrid); (c) Slope 2-A (silt-geotextile); (d) Slope 2-B (silt- geogrid); (e) Slope 3-A (clay-geotextile); (f) Slope 3-B (clay-geogrid).

conductivity (the q/k_s value indicated in Table 3). For $q/k_s < 1$ ($q/k_s = 0.04$ and 0.68 for the reinforced sand and silt slopes, respectively), the inflow flux (i.e., q) was lower than the outflow flux (limited by the k_s of the backfill), resulting in an increase in PWP; however, the soil remained unsaturated when the wetting front passed. For $q/k_s \geq 1$ ($q/k_s = 3.50$ for the reinforced clay slopes), because the inflow flux was higher than the outflow flux, the negative PWP (or matric suction) within the clay backfill was gradually lost with the passage of the wetting front and eventually became completely saturated (Fig. 4e and f).

As rainfall continued, when the steady-state condition or the end of the rainfall event was reached, all cases to some extent exhibited a positive PWP that built up at the bottom of the slope. For Slopes 2-B and 3-B, which had a low drainage capacity, the positive PWP even accumulated up to the top of the slope. The numerical results suggest that installing drainages at the bottom of the slope to minimize the build-up of the positive PWP from the bottom of the slope is important. In addition, under the specified torrential rainfall condition ($q = 350$ mm/

day), the silt and clay slopes of the geogrid cannot effectively drain the infiltrating water. Free drainage conditions may not be assumed for these slopes if the drainage is not properly considered.

Fig. 4 reveals that the PWP profiles were more discontinuous for the nonwoven geotextile-reinforced slopes (Slopes 1-A, 2-A, and 3-A) than for those of the geogrid-reinforced slopes (Slopes 1-B, 2-B, and 3-B). This difference in the PWP profiles is attributed to the capillary barrier effect at the soil–geotextile interface in the geotextile-reinforced slopes. As discussed in the introduction, the capillary barrier effect could increase the water storage of the backfill soils immediately above the nonwoven geotextile beyond the capacity limit that they could ordinarily retain under gravity [36,51]. Consequently, the water in the backfill was momentarily halted and prevented from flowing into the underlying nonwoven geotextile, resulting in excess PWP accumulation at the soil–geotextile interface. Moreover, the capillary barrier effect became more profound with the increase in the fine content in backfill. PWPs in sand, silt, and clay backfills at the topmost geotextile layer increased to −1.5, −2 and +3 kPa, respectively, when wetting fronts were halted above the topmost geotextile layer (Fig. 4).

The capillary barrier effect also affected the infiltration time. For slopes with the same backfill types, the required times for water to pass through geotextile- and geogrid-reinforced slopes were different. The wetting front reached the bottom of the geogrid-reinforced slopes at t = 13.5, 14.8, and 16.8 h for sand, silt, and clay backfills, respectively (Fig. 4). However, the time required for the wetting front to reach the bottom of the geotextile-reinforced slopes was considerably longer (t = 14.3, 18.5, and 21.2 h for sand, silt, and clay backfills, respectively).

Fig. 5 presents the PWP profiles within the reinforced slopes subjected to extremely torrential rainfall (q = 500 mm/day). Under this rainfall condition, the reinforced sand slope with q/k_s = 0.06 remained unsaturated, whereas the reinforced clay slopes with q/k_s = 4.90 were completely saturated when the wetting front reached the bottom of the slope. The reinforced silt slope with a q/k_s value close to 1.0 (q/k_s = 0.96) was nearly saturated when the wetting front reached the bottom of the slope.

Rainfall intensity affects the time taken for the wetting front to advance. For the slope subjected to a higher rainfall intensity, the time required for the wetting front to reach a certain depth was shorter, and the exposure to the same or larger PWP was longer. In addition, the capillary barrier effect still occurred in the geotextile-reinforced slopes under a high rainfall intensity (Slopes 1-C, 2-C, and 3-C in Fig. 5a, c, and e), suggesting that rainfall intensity does not affect the occurrence of the capillary barrier effect.

3.2. Global stability

Fig. 6 presents the variations in the global FS with time (or cumulative rainfall) under different rainfall intensities. Table 5 summarizes the calculated minimum FSs during the rainfall event. The global FS of the reinforced clay slopes initially (t = 0) were considerably higher than those of the reinforced sand and silt slopes. This is because at the beginning of infiltration, the clay backfills exhibited a high initial matric suction (−100 kPa) compared with that of the silt (−12 kPa) and sand (−3.5 kPa) backfills, resulting in a higher soil shear strength and slope stability in the reinforced clay slopes. As rainfall proceeded, the global FS of the reinforced clay slopes substantially decreased due to the loss of matric suction in clay backfills upon rainfall (Fig. 6). The rate of decrease of FS in the reinforced clay slopes was considerably faster than that of the reinforced silt and sand slopes. The minimum global FSs in the reinforced clay slopes were less than those in the reinforced silt and sand slopes, ranging from small to large for reinforced clay, silt, and sand slopes, respectively.

A marked decrease in FS was observed in the geotextile-reinforced clay slope during t = 3.0–5.6 h in Slope 3-A (Fig. 6a) and t = 1.0–4.0 h in Slope 3-C (Fig. 6b). This marked decrease in FS corresponds to the time when excess PWP accumulated at the topmost nonwoven geotextile–backfill interface due to the capillary barrier effect (Figs. 4e and 5e). The capillary barrier effect also resulted in a difference in the front part of the FS curves between the geotextile- and geogrid-reinforced clay slopes (Fig. 6). Once the entire slope was saturated as the wetting front reached the bottom of the slope (t > 21.2 h in Slope 3-A and 18 h in Slope 3-C), the capillary barrier effect became inactive, and the FSs in the geotextile- and geogrid-reinforced clay slopes thus finally converged to a close value.

Both the geotextile-reinforced (Slopes 3-A and 3-C) and geogrid-reinforced (Slopes 3-B and 3-D) clay slopes failed (FS < 1) before the wetting front reached the bottom of the slope because of a significant loss of matric suction in the clay backfills. The slope failure suggests the inadequate drainage or reinforcement capacity of the reinforced clay slopes under the specified rainfall conditions. Remedial measures involving increasing reinforcement tensile strength or installing sand cushions in the reinforced clay slopes were investigated and discussed later.

Regarding the influence of rainfall intensity, the minimum FSs of the reinforced clay slope under different rainfall conditions were close to each other. This is attributed to the low permeability of clay ($q/k_s \gg 1$ for both rainfall intensities), due to which the reinforced clay slope becomes completely saturated under both rainfall conditions. The extra rainfall when q increases from 350 to 500 mm/day becomes surface runoff and does not enter the slope to increase PWP. Although rainfall intensity appears to have little influence on the minimum FS values, the heavier rainfall caused slopes to fail earlier. For example, considering the geotextile-reinforced clay slopes under q = 350 (Slope 3-A) and 500 mm/day (Slope 3-C), Slope 3-C failed at t = 18.5 h, whereas Slope 3-A failed at t = 21 h.

For the reinforced silt slopes, an insignificant difference in FS between the geotextile- and geogrid-reinforced silt slopes (Slope 2-A vs. Slope 2-B and Slope 2-C vs. Slope 2-D) was observed at the front part of the FS curves because the capillary barrier effect was less profound at the silt–geotextile interface than that at the clay–geotextile interface. However, a clear difference in the rear part of the FS curves was observed. For example, the geotextile-reinforced silt slopes exhibited minimum FS = 1.50 (Slope 2-A) and 1.48 (Slope 2-C), whereas the geogrid-reinforced silt slopes (Slopes 2-B and 2-D) exhibited a minimum FS of slightly less than 1.0 (unstable conditions). The failure of Slopes 2-B and 2-D occurred after the wetting front reached the bottom of the slope because of the build-up of a positive PWP at the impervious base (Figs. 4d and 5d). The difference in FS is attributed to the drainage function of the nonwoven geotextile and the lack of drainage function of the geogrid. Because of the drainage function of the geotextile, the geotextile-reinforced silt slopes had FSs higher than those of the geogrid-reinforced silt slopes; consequently, failure did not occur under the specified rainfall conditions.

For the reinforced sand slopes (Slopes 1-A, 1-B, 1-C, and 1-D), the FSs appeared to be consistent with time, suggesting that rainfall infiltration had a minor effect on the FSs. This is because the shear strength of sand exhibited a negligible change with matric suction (Fig. 3c), and the high permeability of sand ($q/k_s << 1$ for both rainfall intensities) prevented the accumulation of a positive PWP. Consequently, the reinforced sand slopes were not completely saturated and could maintain stability under the specified rainfall conditions. This finding supports the use of conventional design methods for GRS structures backfilled with granular soils, in which the effect of PWP is not considered in design by assuming that the granular backfill has a high drainage capacity. Moreover, because sand has a high drainage capacity, the drainage provided by the nonwoven geotextile and rainfall intensity had only a minor effect on the global stability of the reinforced sand slopes because the FSs of Slopes 1-A, 1-B, 1-C, and 1-D were close.

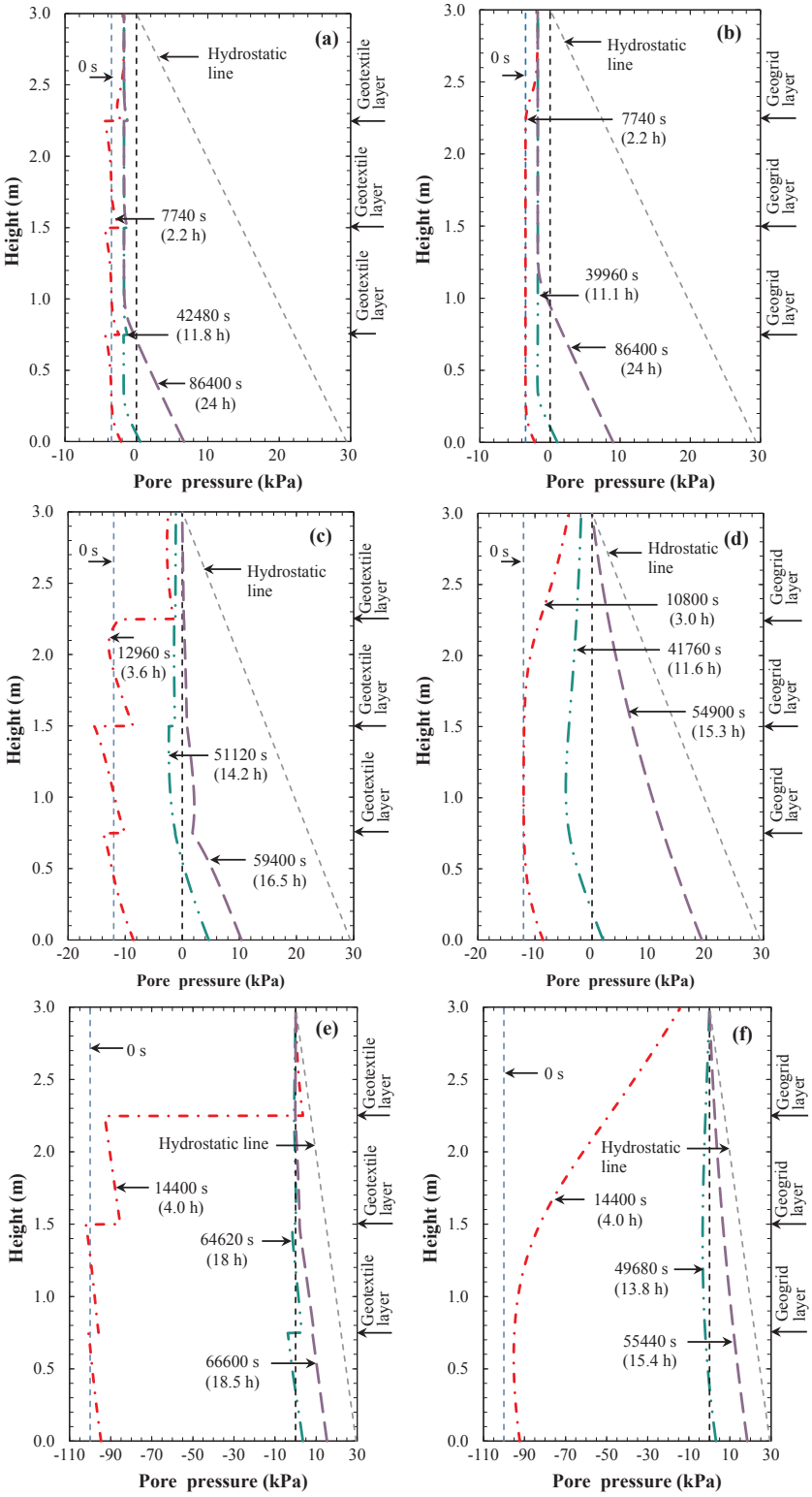

Fig. 5. Porewater pressure profile at a distance of $x = 2.4$ m from the toe of slopes under $q = 500$ mm/day: (a) Slope 1-C (sand-geotextile); (b) Slope 1-D (sand-geogrid); (c) Slope 2-C (silt-geotextile); (d) Slope 2-D (silt- geogrid); (e) Slope 3-C (clay-geotextile); (f) Slope 3-D (clay-geogrid).

3.3. Local stability

Fig. 7 presents the variations in local FS with time (or cumulative rainfall) under different rainfall intensities. The calculated minimum FSs during the rainfall event are summarized in Table 5. A sudden and marked drop in FSs was observed in the geotextile-reinforced clay slopes (Slopes 3-A and 3-C). The FS of Slope 3-A reached its lowest value at $t = 5.6$ and lasted for approximately 1.0 h until $t = 6.5$ h (Fig. 7a), and the FS of Slope 3-C reached its lowest value at $t = 4$ h and lasted for approximately 1.2 h until $t = 5.2$ h (Fig. 7b). These sudden drops in FS corresponded to the development of a positive PWP caused by the capillary barrier effect at the clay–nonwoven geotextile interface (Figs. 4e and 5e), as discussed previously. The occurrence of the minimum local FS in the geotextile-reinforced slopes corresponded to the time at which the maximum PWP occurred in the soil immediately above the topmost nonwoven geotextile due to the capillary barrier effect ($t = 5.6$ h for Slope 3-A and 4 h for Slope 3-C).

The capillary barrier effect had an adverse influence on the local

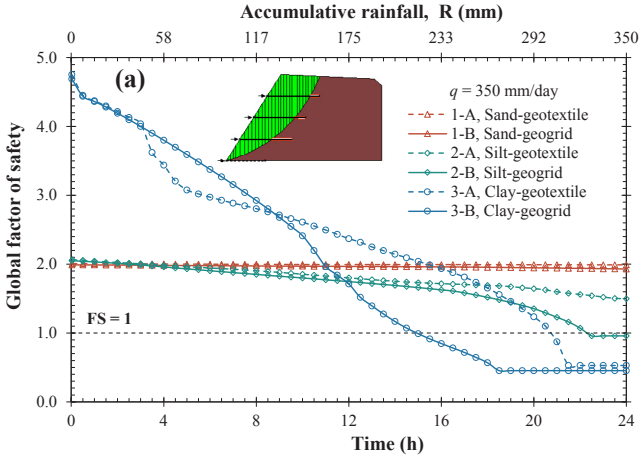

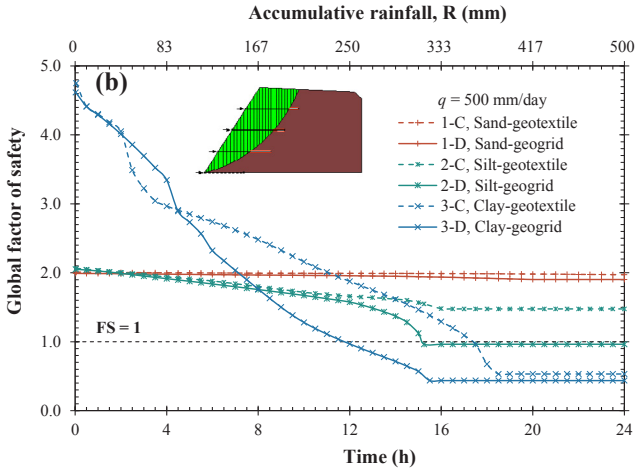

Fig. 6. Comparisons of the global FS of reinforced slopes under: (a) q = 350 mm/day; (b) q = 500 mm/day.

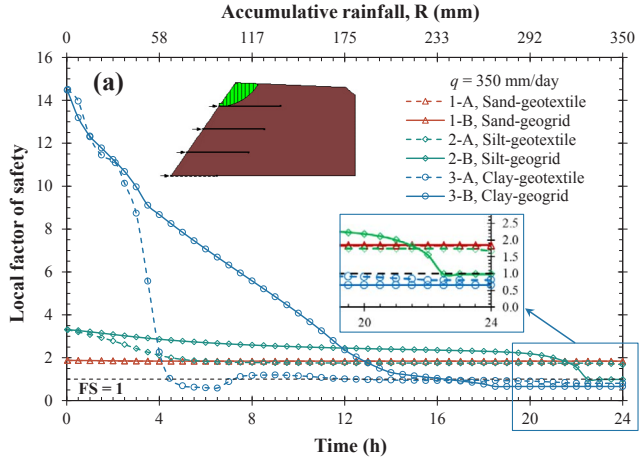

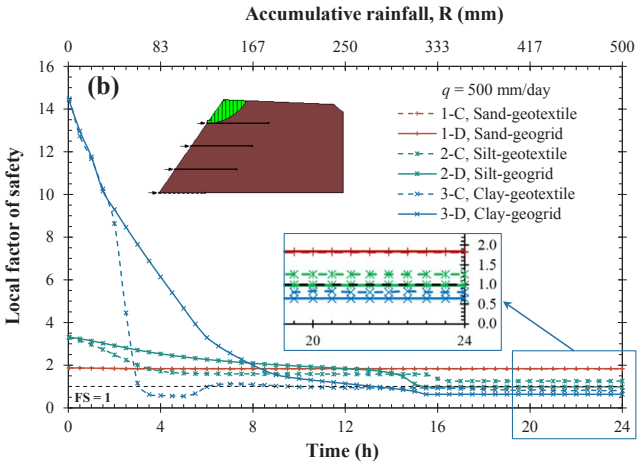

Fig. 7. Comparisons of local FS of reinforced slopes under: (a) q = 350 mm/day; (b) q = 500 mm/day.

stability of the geotextile-reinforced clay slopes (Slopes 3-A and 3-C). The local FS of these slopes decreased to below 1, indicating that the local failure of the interlayer soil sliding along the top reinforcement layer occurred. After the capillary barrier breakthrough, the PWP on the top geotextile layer dissipated, leading to a slight recovery of the FS. Unlike Slopes 3-A and 3-C in which the local failure occurred early, the failure of Slopes 3-B and 3-D (FS slightly less than 1.0) occurred late because of the decrease in the soil–geogrid interface shear strength caused by the loss of matric suction as rainfall continued. Similar to the results for global stability, heavier rainfall caused local slope failure to occur earlier, as is revealed by comparing Fig. 7a and b.

The local FSs of the reinforced silt slopes gradually decreased with rainfall. No marked decrease in FSs in the geotextile-reinforced silt slopes (Slopes 2-A and 2-C) was observed because the capillary barrier effect was less profound in the silt–geotextile interface than in the clay–geotextile interface. Consequently, the capillary barrier effect did not cause the local failure of the geotextile-reinforced silt slopes (Slopes 2-A and 2-C). The geogrid-reinforced silt slopes (Slopes 2-B and 2-D) had minimum local FSs lower than those of the geotextile-reinforced silt slopes (Slopes 2-A and 2-C) because geogrid has no drainage function.

The local stability of the reinforced sand slopes (Slopes 1-A, 1-B, 1-C, and 1-D) was not influenced by rainfall infiltration or the geosynthetic type (with and without drainage function). In addition, rainfall intensity (q = 350 and 500 mm/day) had a negligible effect on the local

Table 5
Summary of calculated minimum factor of safety during rainfall event.

Rainfall intensity	Backfill	Geotextile-reinforced			Geogrid-reinforced		
		Slope	Global FS	Local FS	Slope	Global FS	Local FS
q = 350 (mm/day)	Sand	1-A	1.99	1.84	1-B	1.93	1.84
	Silt	2-A	1.50	1.68	2-B	0.96	0.99
	Clay	3-A	0.53	0.58	3-B	0.45	0.66
	Clay	3-A-5	1.41	0.97	3-B-5	1.18	0.91
	Clay	3-A-15	1.52	1.28	3-B-15	1.36	1.17
	Clay	3-A-25	1.57	1.34	3-B-25	1.51	1.33
	Clay	3-A-35	1.62	1.47	3-B-35	1.58	1.47
q = 500 (mm/day)	Sand	1-C	1.97	1.83	1-D	1.87	1.83
	Silt	2-C	1.48	1.26	2-D	0.96	0.99
	Clay	3-C	0.53	0.54	3-D	0.44	0.64

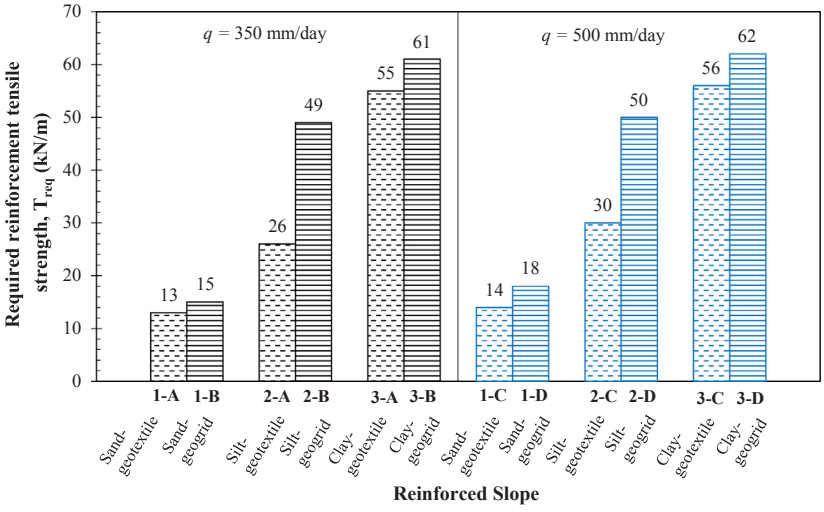

Fig. 8. Required reinforcement tensile strength for reinforced slopes at global FS = 1.3.

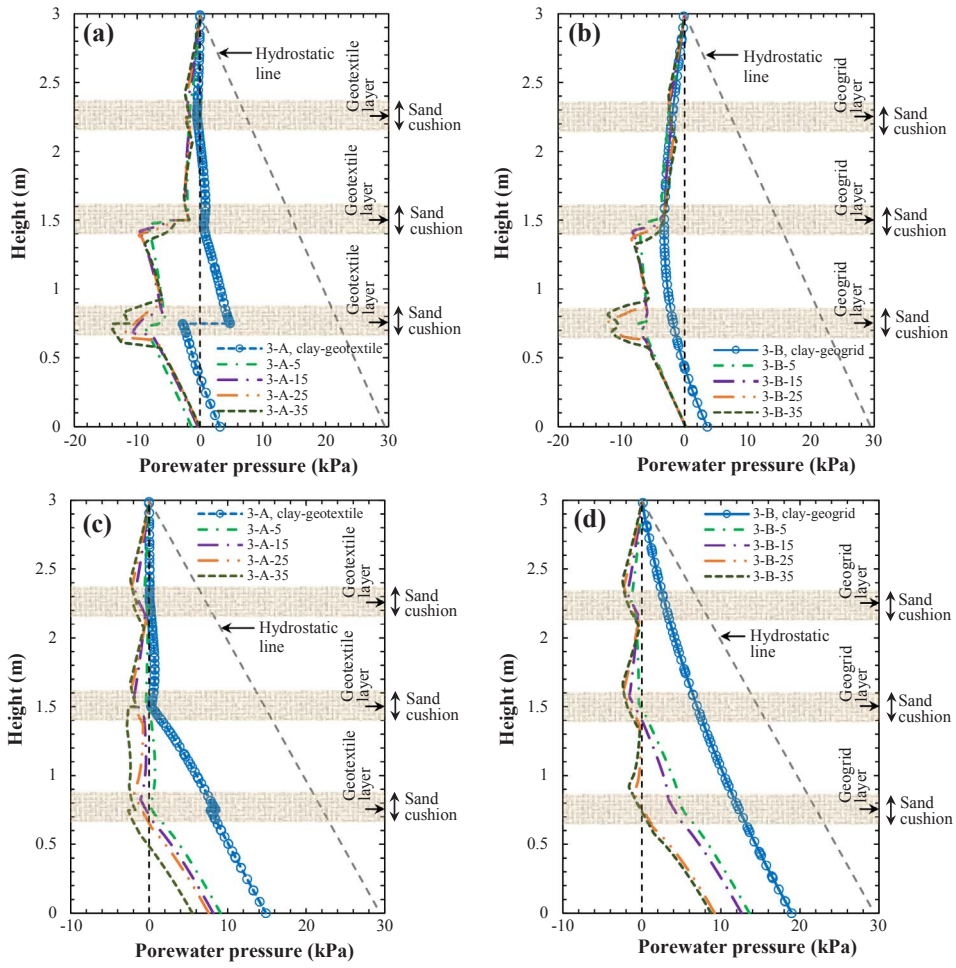

Fig. 9. Porewater pressure profile at a distance of x = 2.4 m from the toe of the slope with different sand cushion thickness when: wetting front reached to the bottom of slope, (a) geotextile reinforced slope, (b) geogrid reinforced slope; at 24 h, (c) geotextile reinforced slope, (d) geogrid reinforced slope.

FS of the reinforced sand slopes. This can be attributed to the high permeability of sand compared to the given rainfall intensities ($q < < k_s$), thus the infiltrating water can be efficiently dissipated and the matric suction did not completely diminish. Similar to the observations in global stability, the minimum local FSs in the reinforced sand slopes were higher than those in the reinforced silt and clay slopes.

3.4. Required reinforcement tensile strength

As previously discussed, the stability of reinforced slopes with marginal backfills (i.e., silt and clay) is lower than that of reinforced slopes with high-quality backfills (i.e., sand) under the specified rainfall conditions. Either the drainage or reinforcement capacities of the reinforced marginal backfill slopes should be improved to enhance the slope stability. The required reinforcement tensile strength T_{req} to achieve the same stability level was evaluated. To determine the T_{req} for

each slope, the input reinforcement tensile strength was gradually increased until a global FS = 1.3 was attained. The value of FS = 1.3 was selected according to the required FS for the reinforced slope in the GRS structure design guidelines [12].

Fig. 8 presents the required reinforcement tensile strength for reinforced slopes at FS = 1.3. T_{req} ranges from small to large in the order of reinforced sand, silt, and clay slopes. The T_{req} values for the reinforced silt and clay slopes to satisfy FS = 1.3 were, respectively, approximately 3 and 4 times larger than that for reinforced sand slopes, irrespective of the reinforcement type and rainfall intensity. This finding was supported by Vahedifard et al. [54], who compared the reinforcement loads of two GRS walls with high-quality and marginal backfills under various surcharge and rainfall levels.

The T_{req} values for geotextile-reinforced slopes are generally less than those for geogrid-reinforced slopes with the same backfill. The difference is attributed to the drainage role played by the nonwoven geotextile, particularly at saturated conditions. Regarding the effect of rainfall intensity on T_{req}, heavier rainfall (q = 500 mm/day) generally requires a higher reinforcement strength to maintain the same stability level. Nevertheless, the difference in T_{req} values for reinforced clay slopes subjected to two specified rainfall conditions was minimal. As previously explained, this is because the maximum amount of water that could infiltrate into the slope is governed by the q/k_s ratio. Because clay has a low hydraulic conductivity ($q/k_s > 1$ for both rainfall intensities), further increase in rainfall intensity does not lead to a significant increase in water infiltration.

4. Evaluation of the effects of sand cushions

4.1. Porewater pressure profile

Fig. 9 presents the PWP profiles of the reinforced clay slopes with different sand cushion thicknesses (i.e., t_s = 0–35 cm) at the time when the wetting front reached the bottom of the slope (Fig. 9a and b) and at the end of the rainfall event at t = 24 h (Fig. 9c and d). Clearly, PWP development in the slopes with sand cushions was less than that in the slopes without sand cushions (Slopes 3-A and 3-B). This result suggests that the inclusion of sand cushions, acting as a drain layer, can effectively facilitate PWP dissipation within the reinforced clay slopes. The difference in PWP between the slopes with and without sand cushions increased with the increase in the sand cushion thickness, particularly at the part of the slope in which the positive PWP developed. Nevertheless, a substantial reduction in PWP was achieved by using 5–15-cm-thick sand cushions, indicating that an optimal sand cushion thickness exists, beyond which the drainage benefits provided by the sand cushion exhibits no significant increase.

As reported in the companion paper [51], the inclusion of sand cushions can also reduce the development of the capillary barrier at the clay–geotextile interface under unsaturated conditions. Thuo et al. [51] reported that sand cushions acted as an intermediate material between the backfill and the nonwoven geotextile, which bridged the gap between two materials with contrasting unsaturated hydraulic characteristics; consequently, the accumulated PWP at the clay–geotextile interface caused by the capillary barrier effect in the soils could be effectively dissipated downward.

4.2. Global and local stabilities

Fig. 10 presents the variation in the global FS of the reinforced clay slopes with different sand cushion thicknesses. At the beginning of the rainfall (t = 0 h), the global FS decreased with an increase in the sand layer thickness. This is because clay backfill had a higher initial suction (−100 kPa) compared with that of sand (−3.5 kPa); thus, the shear strength of clay at the initial conditions was higher than that of sand (see Fig. 3c). Consequently, an increase in the sand cushion thickness initially causes a decrease in the global FS.

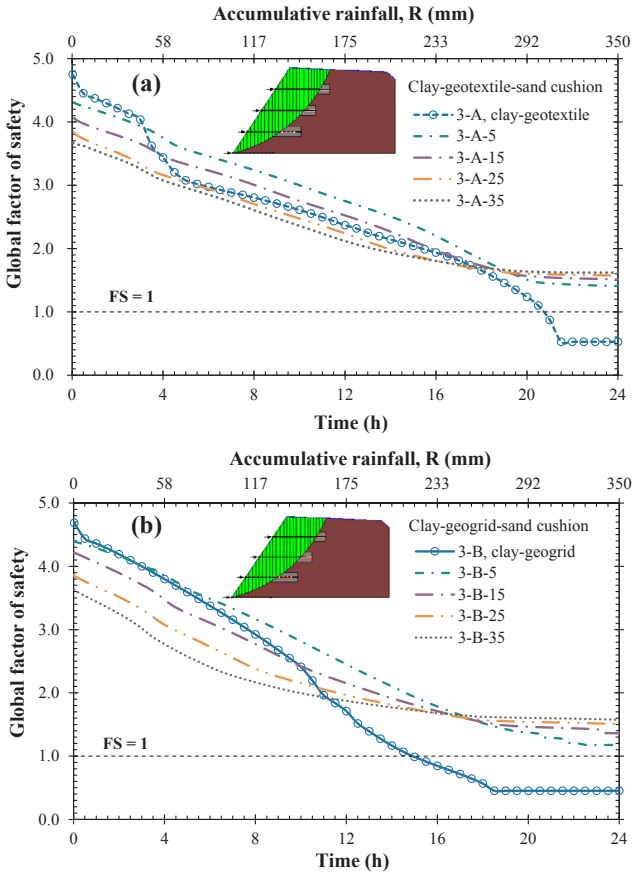

Fig. 10. Variation of global FS of reinforced slopes with different sand cushion thickness: (a) geotextile-reinforced slope; (b) geogrid-reinforced slope.

Because the matric suction was rapidly lost with rainfall, the decreasing rate of FS increased with a decrease in the sand cushion thickness. The FS versus time curves eventually intersected at t = 19 h, and the global FS of the geotextile-reinforced slope with a thicker sand cushion subsequently became higher than that with a thinner one (Fig. 10a). Similar results were observed for the geogrid-reinforced slope when t > 17.5 h (Fig. 10b). At this moment, the entire slope was nearly completely statured, and matric suction had no influence on the soil shear strength. The system stability was enhanced by sand cushions, not only for more efficient drainage capacity (Fig. 9) but also for the higher effective soil shear provided by the sand cushion.

Fig. 11 presents the results of the local FS of the reinforced slopes with different sand cushion thicknesses. Similar to the results in the global FS, a decrease in initial local FS at t = 0 h was observed with an increase in the sand cushion thickness because of the replacement of clay backfill, which had high initial suction with sand cushion layers. For the geotextile-reinforced slopes (Fig. 11a), the local FS substantially dropped because of the capillary barrier effect at the clay–geotextile interface. Because the inclusion of sand cushions can effectively alleviate the capillary barrier effect and prevent the accumulation of PWP at the interface, the local FS of the slopes with sand cushions became higher than that of the slope without sand cushions when the capillary barrier effect developed in Slope 3-A (approximately at t > 4.0 h); thereafter, the local FS of the slopes increased with an increase in the sand cushion thickness.

For the geogrid-reinforced slopes (Fig. 11b), the decrease in the local FS was caused by the loss of matric suction at the soil–geogrid interface. Compared with the slope without sand cushions (Slope 3-B), the local FS decreased at a faster rate in the slopes with sand cushions because of the high permeability of sand allowing a faster and easier rainwater ingress from the slope face. The decrease in the local FS in the

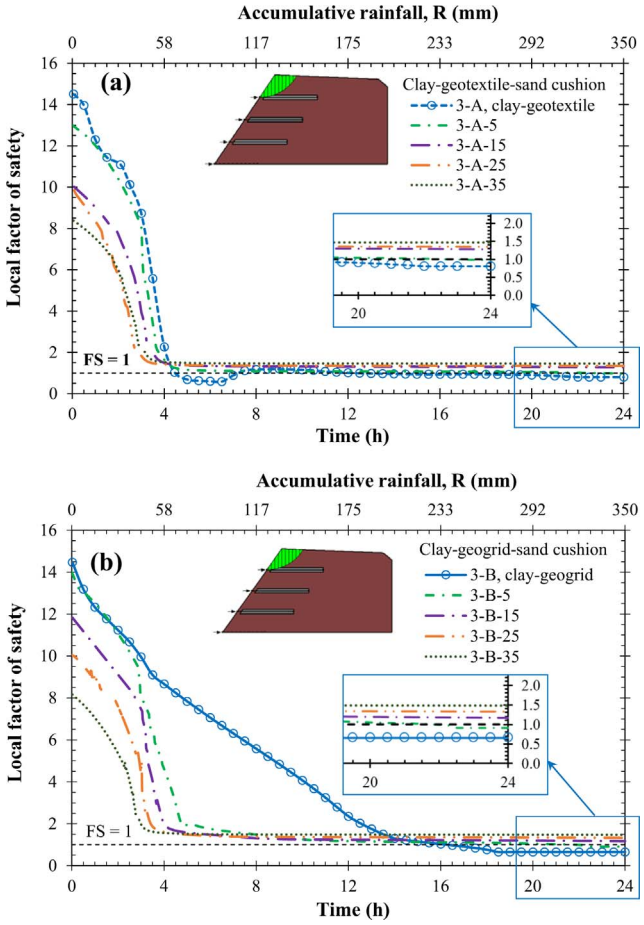

Fig. 11. Variation of local FS of reinforced slopes with different sand cushion thickness: (a) geotextile-reinforced slope; (b) geogrid-reinforced slope.

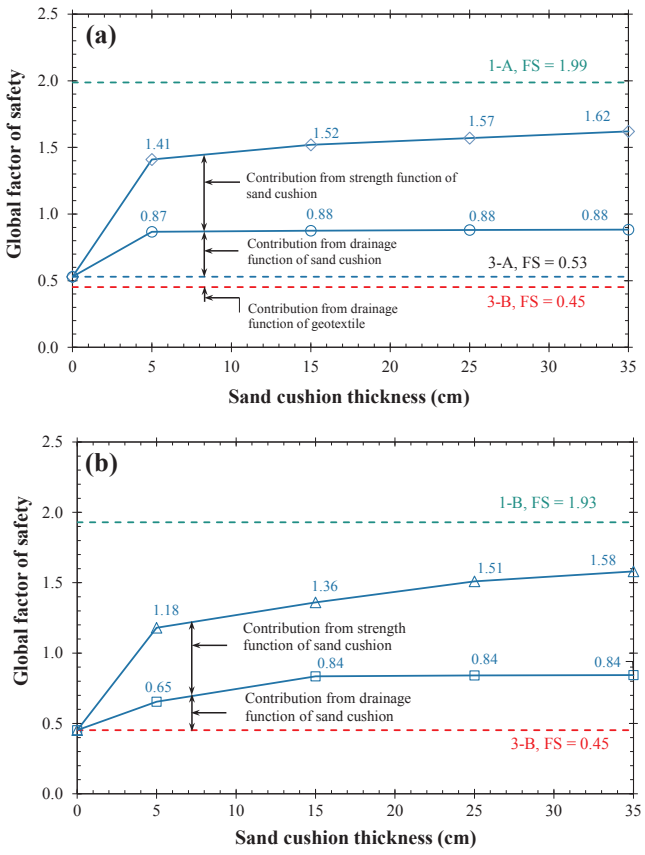

Fig. 12. Contributions of sand cushion in enhancing global FS: (a) geotextile-reinforced slope; (b) geogrid-reinforced slope.

slopes with sand cushions rapidly reached a steady-state condition, and the local FS of the slopes subsequently increased with an increase in the sand cushion thickness. As the local FS of the slope without sand cushions continuously decreased with rainfall, the local FS of the slopes with sand cushions became higher than that of the slope without sand cushions when $t > 16$ h.

Table 5 summarizes the minimum global and local FSs for the slopes with and without sand cushions during the rainfall event. Applying sand cushions effectively enhanced both the local and global FSs by contributing to drainage and strength, thereby enhancing system stability (sand has a higher saturated k_s and ϕ′ than those of clay). An increase in sand cushion thickness leads to an increase in the minimum FS value. As shown in Table 5, a 5-cm sand cushion can improve the global stability of the reinforced clay slopes from unstable (FS = 0.53 and 0.45 for Slopes 3-A and 3-B) to stable conditions (FS = 1.41 and 1.18 for Slopes 3-A-5 and 3-B-5), and a 15-cm sand cushion can improve the local stability from unstable (FS = 0.58 and 0.66 for Slopes 3-A and 3-B) to stable conditions (FS = 1.28 and 1.17 for Slopes 3-A-15 and 3-B-15).

4.3. Quantification of sand cushion contribution

Fig. 12 presents the contributions provided by the strength and drainage functions of sand cushions in enhancing the global FS of the reinforced clay slopes. The global FSs of Slopes 1-A and 1-B are depicted as the upper limits, representing the cases of all clay backfill replaced with sand, whereas the global FS of Slope 3-B is illustrated as the lower limit, representing the cases without sand cushions. To separately quantify the strength and drainage functions of the sand cushion, an additional set of numerical analyses was conducted by inputting the shear strength properties of clay and the hydraulic properties of sand for sand cushions to obtain the sole contribution from the drainage function of the sand cushion. Table 6 summarizes the results of percentage improvement in slope stability with respect to the FS of the lower limit.

For the geotextile-reinforced slopes (Fig. 12a), the global FS clearly increased with an increase in the sand cushion thickness. The percentage improvements contributed by the drainage of the geotextile and the drainage and strength of the sand cushion were 17%, 74–78%, and 120–163%, respectively (Table 6). The geogrid-reinforced slopes also exhibited a similar trend of increasing FS with the sand cushion thickness (Fig. 12b). The percentage improvements contributed by the drainage and strength of the sand cushion were 45–87% and 116–163%, respectively (Table 6). Notably, the strength of the sand cushion had a larger contribution in enhancing the global FS than the drainage of the sand cushion and geotextile. The contribution from the strength of the sand cushion increased as the sand cushion thickness increased, with the upper bound considered to be the FS of the reinforced sand slope. The contribution provided by the drainage of the sand cushion was not substantially affected by the sand cushion thickness. An increase in the sand cushion thickness beyond 5 cm in the geotextile-reinforced clay slope and 15 cm in the geogrid-reinforced clay slopes did not further increase the contribution provided by the drainage of the sand cushion.

Fig. 13 presents the results of the contribution of sand cushions in enhancing the local FS of the reinforced clay slopes. The local FS increased with an increase in the sand cushion thickness in both the geotextile- and geogrid-reinforced slopes. For the geotextile-reinforced slopes, the percentage improvements contributed by the drainage and strength of the sand cushion were 51–71% and 15–80%, respectively (Table 7). The drainage provided by the sand cushion had a larger

Table 6
Summary of percentage contributions of sand cushion to global FS.

Sand cushion thickness (cm)	Geotextile-reinforced				Geogrid-reinforced		
	Slope	Geotextile drainage (%)	Sand cushion drainage (%)	Sand cushion strength (%)	Slope	Sand cushion drainage (%)	Sand cushion strength (%)
0	3-A	17	–	–	3-B	–	–
5	3-A-5	17	74	120	3-B-5	45	116
15	3-A-15	17	76	143	3-B-15	85	116
25	3-A-25	17	78	152	3-B-25	86	148
35	3-A-35	17	78	163	3-B-35	87	163

Note: Percentage improvement with respect to the FS of slope 3-B

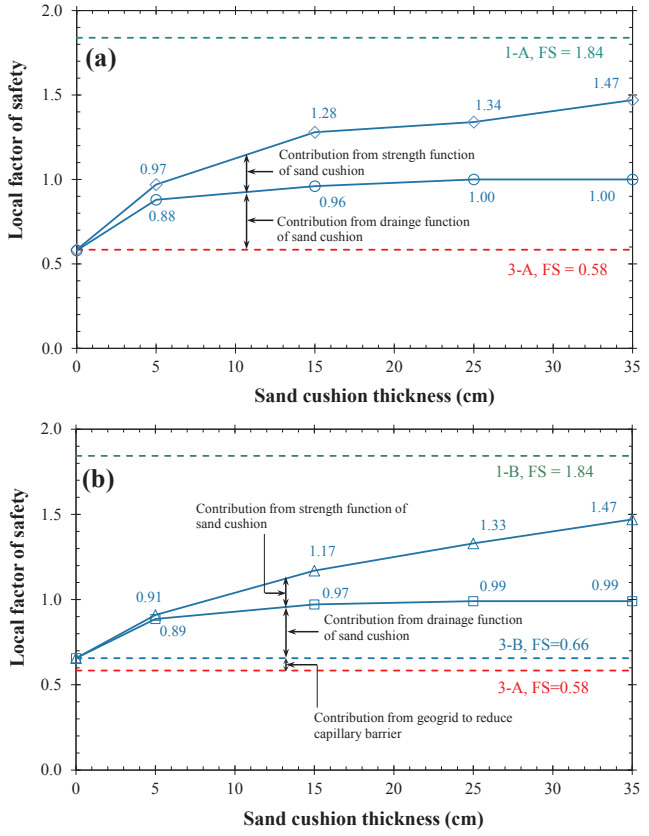

Fig. 13. Contributions of sand cushion in enhancing local FS: (a) geotextile-reinforced slope; (b) geogrid-reinforced slope.

contribution in enhancing the local FS than the strength of the sand cushion because sand cushions can facilitate the dissipation of the positive PWP accumulated at the soil–geotextile interface. For the geogrid-reinforced slopes, the percentage improvements contributed by the geogrid to reduce capillary barrier effect and the drainage and strength of the sand cushion were 12%, 39–57%, and 4–82%, respectively (Table 7). Similar to the observation regarding global stability, an increase in the sand cushion thickness beyond 5 cm in the geotextile-reinforced clay slopes and 15 cm in the geogrid-reinforced clay slopes did not further increase the contribution from the drainage of the sand cushion.

An optimal sand cushion thickness of 15 cm was determined by this study. Considering a vertical reinforcement spacing of 75 cm in the slope model applied in this study (Fig. 2), a 15-cm sand cushion is equivalent to replacing 20% of marginal backfill with sand. This value was determined on the basis that a 15-cm sand cushion can not only achieve its maximum drainage contribution but is also adequate to prevent local and global failures in both geotextile- and geogrid-reinforced clay slopes under the specified rainfall conditions.

5. Design implications

The study findings reveal that the loss of matric suction and development of a capillary barrier effect within the marginal backfill could have a negative impact on both the global and local stabilities of reinforced clay slopes. In addition, the study indicates that the reinforced marginal soil slopes cannot effectively drain the infiltrating water under torrential rainfall (q = 350 mm/day). Free drainage conditions may not be assumed for these slopes if the drainage is not properly considered. Consequently, GRS structures with cohesive soil as an alternative backfill material should be designed with special caution to prevent the aforementioned adverse effects.

To guarantee a satisfactory and safe design, the numerical procedures presented and discussed in this paper can be applied to evaluate the stability of reinforced marginal soil slopes subject to heavy rainfall. First, a design rainfall intensity should be selected on the basis of the annual exceedance probability or the return period specified in the regional code for hydrological design. Subsequently, transient infiltration analyses should be performed by inputting the specified rainfall condition to obtain PWP information. LE analyses based on framework of unsaturated soil mechanics can be conducted using the estimated PWP distribution obtained from the transient infiltration analyses to evaluate the variation in FS with rainfall. If the minimum FS is less than the required value under the specified rainfall condition, the measures

Table 7
Summary of percentage contributions of sand cushion to local FS.

Sand cushion thickness (cm)	Geotextile-reinforced			Geogrid-reinforced			
	Slope	Sand cushion drainage (%)	Sand cushion strength (%)	Slope	Geogrid to reduce capillary barrier (%)	Sand cushion drainage (%)	Sand cushion strength (%)
0	3-A	–	–	3-B	12	–	–
5	3-A-5	51	15	3-B-5	12	39	4
15	3-A-15	64	55	3-B-15	12	54	34
25	3-A-25	71	58	3-B-25	12	57	58
35	3-A-35	71	80	3-B-35	12	57	82

Note: Percentage improvement with respect to the FS of slope 3-A

to improve the drainage and reinforcement capacities of the reinforced slopes can be proposed (e.g., enhancing the drainage design, increasing the reinforcement tensile strength or layers, and installing sand cushions). The effectiveness of these measures can be assessed by following the same numerical procedures. Furthermore, based on the suggested procedures, design charts for reinforced slopes with various geometries, backfills, and geosynthetic systems subject to diverse rainfall intensities can be developed to facilitate the design of GRS structures that can withstand heavy rainfall.

6. Conclusions

This paper presents a numerical study investigating the hydraulic response and stability of geosynthetic-reinforced soil slopes subject to rainfall. A series of numerical simulations of unsaturated slopes with various backfill–reinforcement–drainage systems were performed by comprehensively considering the combined effect of backfill, reinforcement type, and rainfall intensity. The effectiveness of sand cushions in improving the drainage and stability of the reinforced clay slopes was also assessed. The following conclusions were drawn from the results presented in this study:

- The matric suction had a significant influence on the stability of the reinforced clay slopes. The contribution of matric suction in enhancing slope stability was initially high; however, as rainfall proceeded, the global FS of the reinforced clay slope decreased substantially due to the loss of matric suction.
- The capillary barrier effect affected the stability of the geotextile-reinforced clay slopes. The wetting front momentarily halted and a positive PWP accumulated at the interface between the soil and the underlying geotextile. The local FS of the geotextile-reinforced clay slopes decreased to below 1, indicating that the local failure occurred due to the capillary barrier effect. The adverse influence of the capillary barrier effect on local stability was more profound in cohesive soil than in granular soil.
- Both the global and local stabilities of reinforced sand slopes were minimally influenced by the geosynthetic type (with and without drainage function) and rainfall intensity. Because sand has a high permeability and its shear strength is insensitive to changes in matric suction, the FSs of the reinforced sand slopes appeared to be consistent with rainfall infiltration.
- The minimum global and local FSs ranged from small to large in the order of reinforced clay, silt, and sand slopes.
- The required reinforcement tensile strengths for the reinforced silt and clay slopes to achieve the same stability level (FS = 1.3) were, respectively, approximately 3 and 4 times larger than that for reinforced sand slopes.
- The saturation and build-up of positive PWPs within the reinforced slopes depends on the q/k_s ratio and drainages at the bottom of the slope. Numerical results indicated that reinforced marginal soil slopes without bottom drainage cannot effectively drain the infiltrating water under torrential rainfall conditions. Free drainage conditions may not be assumed for these slopes if the drainage is not properly considered.
- The inclusion of sand cushions, which provide both strength and drainage functions, can effectively enhance the slope stability of reinforced clay slopes. The system stability increased with the increase in sand cushion thickness.
- The improvement in system stability that resulted from the drainage function of the sand cushion reached a maximum value when the sand cushion thickness increased beyond 15 cm, whereas the improvement in system stability that resulted from the strength function of the sand cushion continued to increase with the increase in the sand cushion thickness. An optimal sand cushion thickness of 15 cm (replacing 20% of marginal backfill with sand) was determined in this study.

Acknowledgements

The financial support for this research was from the Ministry of Science and Technology of Taiwan under grant no. NSC102-2221-E-011-057-MY3. The financial supports for the second and fourth authors during their graduate study were provided by the Taiwan Ministry of Education under the grant for “Aim for the Top-Tier University Project”. These financial supports are gratefully acknowledged.

References

[1] AASHTO. Standard specifications for highway bridges. Washington, D.C., with interims: American Association of State Highway and Transportation Officials; 2002.
[2] Abdi MR, Sadrnejad A, Arjomand MA. Strength enhancement of clay by encapsulating geogrids in thin layers of sand. Geotext Geomembr 2009;27(6):447–55.
[3] Abdi MR, Zandieh AR. Experimental and numerical analysis of large scale pull out tests conducted on clays reinforced with geogrids encapsulated with coarse material. Geotext Geomembr 2014;42(5):494–504.
[4] Balakrishnan S, Viswanadham BVS. Performance evaluation of geogrid reinforced soil walls with marginal backfills through centrifuge model tests. Geotext Geomembr 2016;44(1):95–108.
[5] Berg R, Christopher BR, Samtani N. Design of mechanically stabilized earth walls and reinforced soil slopes. Report no. FHWA-NHI-10-024, vols. I and II. Washington, DC, USA: National Highway Institute, Federal Highway Administration; 2009.
[6] Blake JR, Renaud JP, Anderson MG, Hencher SR. Prediction of rainfall-induced transient water pressure head behind a retaining wall using a high-resolution finite element model. Comput Geotech 2003;30(6):431–42.
[7] Bouazza A, Zornberg JG, McCartney J, Singh R. Unsaturated geotechnics applied to geoenvironmental engineering problems involving geosynthetics. Eng Geol 2013;165:143–53.
[8] Cai F, Ugai K. Numerical analysis of rainfall effects on slope stability. Int J Geomech 2004;4(2):69–78.
[9] Chen JF, Yu SB. Centrifugal and numerical modeling of a reinforced lime-stabilized soil embankment on soft clay with wick drains. Int J Geomech 2011;11(3):167–73.
[10] Christopher BR, Zornberg JG, Mitchell JK. Design guidance for reinforced soil structures with marginal soil backfills. Proceedings, sixth international conference on geosynthetics, Atlanta, Georgia, vol. 2. 1998. p. 797–804.
[11] Eigenbrod KD, Locker JG. Determination of friction values for the design of side slope lined or protected with geosynthetics. Can Geotech J 1987;24:509–19.
[12] Elias V, Christopher BR, Berg R. Mechanically stabilized earth walls and reinforced soil slopes design and construction guidelines. Report No. FHWA-NHI-00-043. Washington, D.C.: National Highway Institute, Federal Highway Administration; 2001.
[13] Fredlund DG. Unsaturated soil mechanics in engineering practice. J Geotech Geoenviron Eng 2006;132(3):286–321.
[14] Fredlund DG, Morgenstern NR. Stress-state variables for unsaturated soils. J Geotech Geoenviron Eng 1977;103(GT5):447–66.
[15] Garcia EF, Gallage CPK, Uchimura T. Function of permeable geosynthetics in unsaturated embankments subjected to rainfall infiltration. Geosynth Int 2007;14(2):89–99.
[16] Geo-Slope. Stability modeling with SLOPE/W. Calgary, Canada: GEO-SLOPE International Ltd; 2007.
[17] Geo-slope. Seepage modeling with SEEP/W 2007. Calgary, Canada: GEO-SLOPE International Ltd; 2009.
[18] Glendinning S, Jones C, Pugh R. Reinforced soil using cohesive fill and electrokinetic geosynthetics. Int J Geomech 2005;5(2):138–46.
[19] Griffiths DV, Lu N. Unsaturated slope stability analysis with steady infiltration or evaporation using elasto-plastic finite elements. Int J Numer Anal Meth Geomech 2005;29(3):249–67.
[20] Hamid TB, Miller GA. Shear strength of unsaturated soil interfaces. Can Geotech J 2009;46(5):595–606.
[21] Hatami K, Esmaili D, Chan EC, Miller GA. Moisture reduction factors for shear strength of unsaturated reinforced embankments. Int J Geomech 2016:D4016001.
[22] Holtz RD, Kovacs WD. An introduction to geotechnical engineering. Englewood Cliffs, N.J: Prentice-Hall; 1981.
[23] Iryo T, Rowe RK. Numerical study of infiltration into a soil-geotextile column. Geosynth Int 2004;11(5):377–89.
[24] Iryo T, Rowe RK. Hydraulic behaviour of soil-geocomposite layers in slopes. Geosynth Int 2005;12(3):145–55.
[25] Iryo T, Rowe RK. Infiltration into an embankment reinforced by nonwoven geotextiles. Can Geotech J 2005;42(4):1145–59.
[26] Kim WS, Borden R. Numerical simulation of MSE wall behavior induced by surface-water infiltration. J Geotech Geoenviron Eng 2013;139(12):2110–24.
[27] Khalili N, Geiser F, Blight G. Effective stress in unsaturated soils: review with new evidence. Int J Geomech 2004;4(2):115–26.
[28] Koerner RM, Koerner GR. A data base, statistics and recommendations regarding 171 failed geosynthetic reinforced mechanically stabilized earth (MSE) walls. Geotext Geomembr 2013;40:20–7.
[29] Koutsourais M, Sandri D, Swan R. Soil interaction characteristics of geotextiles and geogrids. Proceedings, sixth international conference on geosynthetics, Atlanta, Georgia, vol. 2. 1998. p. 739–44.
[30] Leshchinsky D. On global equilibrium in design of geosynthetic reinforced wall. J

Geotech Geoenviron Eng 2009;135(3):309–15.
[31] Lin C-Y, Yang K-H. Experimental study on measures for improving the drainage efficiency of low-permeability and low-plasticity silt with nonwoven geotextile drains. J Chinese Inst Civil Hydraul Eng 2014;26(2):71–82.
[32] Liu CN, Yang KH, Ho YH, Chang CM. Lessons learned from three failures on a high steep geogrid-reinforced slope. Geotext Geomembr 2012;34:131–43.
[33] Lu N, Likos WJ. Unsaturated soil mechanics. John Wiley & Sons; 2004.
[34] Martin JP, Koerner RM, Whitty JE. Experimental friction evaluation of slippage between geomembranes, geotextiles and soils. In: Proceedings, international conference on geomembranes. Denver: IFAI; 1984.
[35] Matsumaru T, Uzuoka R. Three-phase seepage-deformation coupled analysis about unsaturated embankment damaged by earthquake. Int J Geomech 2016;16(5). http://dx.doi.org/10.1061/(ASCE)GM.1943-5622.0000699.
[36] McCartney JS, Zornberg JG. Effects of infiltration and evaporation on geosynthetic capillary barrier performance. Can Geotech J 2010;47(11):1201–13.
[37] Mendes J, Toll D. Influence of initial water content on the mechanical behavior of unsaturated sandy clay soil. Int J Geomech 2016. http://dx.doi.org/10.1061/(ASCE)GM.1943-5622.0000594.
[38] Mitchell JK, Zornberg JG. Reinforced soil structures with poorly draining backfills. Part II: case histories and applications. Geosynth Int 1995;2(1):265–307.
[39] NCMA. Design manual for segmental retaining walls. Virginia, USA: Herndon; 2010.
[40] Oh WT, Vanapalli SK. Interpretation of the bearing capacity of unsaturated fine-grained soil using the modified effective and the modified total stress approaches. Int J Geomech 2013;13(6):769–78.
[41] Portelinha FHM, Bueno BS, Zornberg JG. Performance of nonwoven geotextile-reinforced walls under wetting conditions: laboratory and field investigations. Geosynth Int 2013;20(2):90–104.
[42] Portelinha FHM, Zornberg JG. Development of capillary barriers during water infiltration in a geotextile-reinforced soil wall. In: 10th International conference of geosynthetics, Berlin, Germany; 2014. p. 1–7.
[43] Raisinghani DV, Viswanadham BVS. Evaluation of permeability characteristics of a geosynthetic-reinforced soil through laboratory tests. Geotext Geomembr 2010;28(6):579–88.
[44] Raisinghani DV, Viswanadham BVS. Centrifuge model study on low permeable slope reinforced by hybrid geosynthetics. Geotext Geomembr 2011;29(6):567–80.
[45] Raja J, Dixon N, Frost M, Zornberg JG. Designing with marginal fills: understanding and practice. In: Proc., 5th European geosynthetics congress.; 2012. p. 460–5.
[46] Riccio M, Ehrlich M, Dias D. Field monitoring and analyses of the response of a block-faced geogrid wall using fine-grained tropical soils. Geotext Geomembr 2014;40(2):127–38.
[47] Richards LA. Capillary conduction of liquids through porous mediums. Physics 1931;1:318–33.
[48] Sheng D. Review of fundamental principles in modelling unsaturated soil behaviour. Comput Geotech 2011;38(6):757–76.
[49] Spencer E. A method of analysis of the stability of embankments assuming parallel inter-slice forces. Geotechnique 1967;24(4):661–5.
[50] Sun D, Zhang J, Gao Y, Sheng D. Influence of suction history on hydraulic and stress-strain behavior of unsaturated soils. Int J Geomech 2015. http://dx.doi.org/10.1061/(ASCE)GM.1943-5622.0000602.
[51] Thuo JN, Yang KH, Huang CC. Infiltration into unsaturated reinforced slopes with nonwoven geotextile drains sandwiched in sand layers. Geosynth Int 2015;22(6):457–74.
[52] Unnikrishnan N, Rajagopal K, Krishnaswamy NR. Behaviour of reinforced clay under monotonic and cyclic loading. Geotext Geomembr 2002;20(2):117–33.
[53] Vahedifard F, Leshchinsky D, Mortezaei K, Liu N. Effective stress-based limit equilibrium analysis for homogeneous unsaturated slopes. Int J Geomech 2016;16(6):D4016003.
[54] Vahedifard F, Mortezaei K, Leshchinsky BA, Leshchinsky D, Lu N. Role of suction stress on service state behavior of geosynthetic-reinforced soil structures. Transp Geotech 2016;8:45–8.
[55] Vahefifard F, Robinson JD. Unified method for estimating the ultimate bearing capacity of shallow foundations in variably saturated soils under steady flow. J Geotech Geoenviron Eng 2016;142(4):04015095.
[56] Valentine RJ. An assessment of the factors that contribute to the poor performance of geosynthetic-reinforced earth retaining walls. In: Proc., design and practice of geosynthetic-reinforced soil structures. United States of America; DEStech Publications, Inc.; 2013. p. 318–27.
[57] Vanapalli SK, Fredlund DG, Pufahl DE, Clifton AW. Model for the prediction of shear strength with respect to soil suction. Can Geotech J 1996;33(3):379–92.
[58] Vanapalli SK, Mohamed FMO. Bearing capacity and settlement of footings in unsaturated sands. Int J Geomater 2013;5(1):595–604.
[59] van Genuchten MTh. A closed-form equation for predicting the hydraulic conductivity of unsaturated soils. Soil Sci Soc Am J 1980;44:892–8.
[60] Yang K-H, Yalew WM, Nguyen MD. Behavior of geotextile-reinforced clay with a coarse material sandwich technique under unconsolidated-undrained triaxial compression. Int J Geomech 2016;16(3):04015083.
[61] Yoo C, Jung H-Y. Case history of geosynthetic reinforced segmental retaining wall failure. J Geotech Geoenviron Eng 2006;132(12):1538–48.
[62] Zhan T, Ng C. Analytical analysis of rainfall infiltration mechanism in unsaturated soils. Int J Geomech 2004;4(4):273–84.
[63] Zhang LL, Fredlund DG, Fredlund MD, Wilson GW. Modeling the unsaturated soil zone in slope stability analysis. Can Geotech J 2014;51:1384–98.
[64] Zornberg JG, McCartney JS, Bouazza A. Geosynthetic capillary barriers: current state of knowledge. Geosynth Int 2010;17(5):273–300.
[65] Zornberg JG, Mitchell JK. Reinforced soil structures with poorly draining backfills. part i:reinforcement interactions and functions. Geosynth Int 1994;1(2):103–48.
[66] Zornberg JG, Sitar N, James KM. Limit equilibrium as basis for design of geosynthetic reinforced slopes. J Geotech Geoenviron Eng, ASCE 1998;124(8):684–98.
[67] Hatami K, Esmaili D. Unsaturated soil-woven geotextile interface strength properties from small-scale pullout and interface tests. Geosynth Int 2015;22(2):161–72.